Available online at www.sciencedirect.com
ScienceDirect
Engineering Failure Analysis 16 (2009) 656–668
ENGINEERING FAILURE ANALYSIS
www.elsevier.com/locate/engfailanal

Study of fatigue damage in wind turbine blades

J.C. Marín *, A. Barroso, F. París, J. Cañas

School of Engineering, University of Seville, Camino de los Descubrimientos s/n, 41092 Seville, Spain

Available online 29 February 2008

Abstract

The inspection of damages detected in some blades of 300 kW wind turbines revealed that the nature of these damages was probably due to a fatigue mechanism. The causes that had originated the failure (superficial cracks, geometric concentrator, abrupt change of thickness) have been studied, verifying, by means of the simplified evaluation procedure of fatigue life of the "Germanischer Lloyd" (GL) standard, that these causes can explain the failure detected in the period of time in which it happened.

Keywords: Blade failures; Composites; Fatigue life

1. Introduction

The objective of the present work is the study of the damages detected in the blades of 300 kW wind turbines. These damages, consisting of cracks located in the joining zone of the blade with the root, appeared over short periods of time and systematically in blades in which fatigue loads were more severe. Similar damages appeared also, but over longer periods of time, in blades under more benign fatigue conditions. In any case, these periods were inferior to the design life of the blades (20 years). In this work, the reasons lying behind the damages detected are studied, to be used as a basis for repairing similarly affected blades.

First, a complete inspection of the damaged zone of the blade was carried out, cutting this damaged zone to evaluate the nature of the damage and to observe the inner structure of the zone. The correct correspondence of the structure of the laminates with that established at design as well as the existence of possible defects of manufacture is verified. The results of this visual inspection allow a qualitative estimation of the causes which could originate the appearance of the cracks to be performed.

The quantitative justification of the viability of the appearance of the failure observed, in the period of time detected, has been carried out using the simplified model of the GL standard.

* Corresponding author. Tel.: +34 954487299; fax: +34 954461637.
E-mail address: jcmarin@esi.us.es (J.C. Marín).

1350-6307/$ - see front matter © 2008 Elsevier Ltd. All rights reserved.
doi:10.1016/j.engfailanal.2008.02.005

2. Visual inspection of the cracks and analysis of laminates

A picture of the typical damage found in a blade, in the form of cracks on the external surface, is presented in Fig. 1. The crack is located in the transition zone between the root of the blade and the zone of aerofoil profile. The cross-sectional section of the blade in the aerodynamic zone is a thin-walled section that reproduces the aerofoil profile and presents a vertical partition (denominated spline) that divides the section into two cells: leading edge and trailing edge (Fig. 2). The cross section in the root zone is practically cylindrical.

The transition between the root zone and the aerodynamic zone is made in such a way that the cylindrical root geometry is progressively transformed into the cell of the leading edge that constitutes the resistant part of the section. The cell of the trailing edge is closed in the zone of transition by means of an element triangular in shape, constituted by a laminate of low resistance, an element which we will refer to in what follows as cover. As can be observed in Fig. 1, the crack extends throughout both the union cover-root and the transition root-aerodynamic zone.

In order to have a visual inspection of the failure area, it is divided into slices of 2–3 cm of width, as shown in Fig. 3a and b, so that the progression of the internal damage can be observed. A detail of the damaged area at slice number 7 is shown in Fig. 3c, whereas those areas corresponding to slices number 6 (left) and number 5 (right) are shown in Fig. 3d.

Although the evolution of damage is difficult to establish, the crack observed in the inspection (see Fig. 1) is formed by several well differentiated parts: (a) the part that runs through the cover (slices 8 and 9), which affects the whole thickness of a laminate without resistant function, (b) the continuation of this part on slice 7 which only affects the external layers of the laminate, with breaking of unidirectional fibres and multiple delaminations (as can be observed in Fig. 3c), (c) the part corresponding to slices 5 and 6 in which the whole

Fig. 1. Location of the cracks on the surface of a blade.

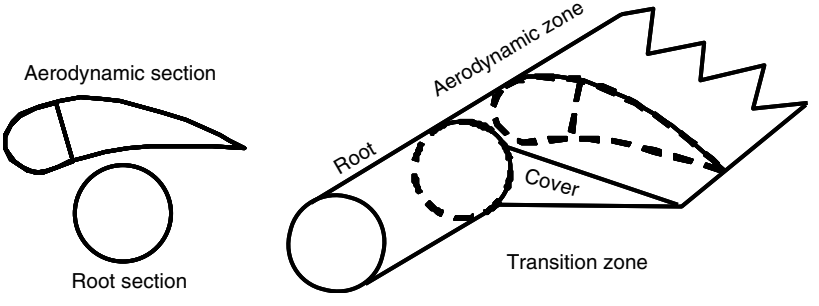

Fig. 2. Scheme of the blade geometry.

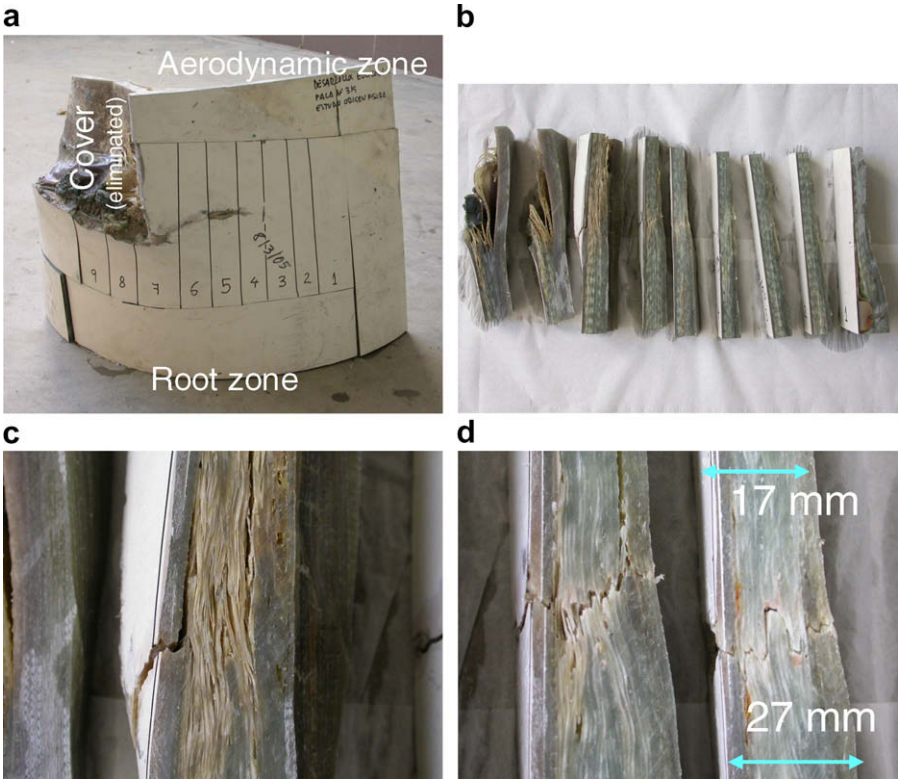

Fig. 3. Details of the internal damage suffered by the blade.

thickness is damaged (as observed in Fig. 3d), and finally (d) slice 4 where the actual crack front is located, as no appreciable damage is observed at the side facing slice 3.

The following information can be deduced from the inspection of the samples:

- An a *posteriori* lamination over the gel coat on the external surface and centered in the area of the crack (see Fig. 3d) can be observed.
- An abrupt change in the thickness of the laminate exists in the area of the crack (see Fig. 3b and d for more detail) the difference of thickness being in some cases (slice 5) up to 10 mm, from 17 mm to 27 mm, over a distance of only 150 mm.
- The presence of areas with lack of resin (see Figs 3b and c).
- A debonding is observed between the spline and the aerodynamic walls (when the whole set is looked at from the upper part).

Calcinations of laminate samples from slice 5 were carried out in a muffle oven at 600 °C for 90 min to obtain the real stacking sequence on both sides of the crack. After the calcination of the resin, the layers defining the laminate are shown in Fig. 4.

Fig. 4. Stacking sequence of the laminate.

Table 1
Laminate obtained in the calcinated samples

Laminate of root part		1	1	13	1	4	1	1	3	1
	GEL	MAT	TRIAX	NUFF	BIAX	NUFF	MAT	TRIAX	BIAX	TRIAX

The stacking sequence observed after the calcinations is shown in Table 1, where MAT indicates layers of short fibre randomly distributed, NUFF represents unidirectional layers oriented at 0° with respect to the longitudinal direction, TRIAX represents triaxial layers 90/45/−45, BIAX represents biaxial layers 0/90 and/or 45/−45, and GEL denotes the external layer of gel coat.

The most noticeable result is the difference in the number of unidirectional layers (in a proportion of 17–10) from the root zone to the aerodynamic area. Also noticeable is the presence of several biaxial 0/90 layers and one triaxial layer inside the root part that do not appear in the aerodynamic part.

Comparing the laminate found in the calcinated samples with the laminate that is described in the lamination manual, an excellent agreement is observed in the laminate of the aerodynamic part, whereas the laminate of the root part presents in the sample several additional layers of NUFF in comparison with that prescribed in the lamination manual. This increment of layers observed may be motivated by the existence of overlap in circumferential direction in the disposition of the layers in the laminate of the root.

3. Evaluation of the causes of damage

After the visual inspection carried out, the causes most likely to have played a significant role in the origin of the detected damage are: the abrupt change of thickness observed, the local geometry of stress concentrator in the transition area, and the observed defects of manufacture of the blade. These factors are discussed separately in what follows.

3.1. Abrupt change of thickness

The most damaged zone from a structural point of view is the one between slices 5 and 6, in which the damage affects the whole thickness of the laminate, whereas the crack does not cross the whole thickness in slice 7.

It is in these slices (5 and 6) that, after the inspection carried out in Section 2, a more marked transition in thickness can be observed (Fig. 3). This abrupt change of thickness produces an eccentricity in the transmission of the load, generating bending moments that make the laminate not work uniformly over the whole thickness. Additionally, the unidirectional layers that are present in both laminates suffer misalignment in the longitudinal orientation of the fibre. This misalignment, under compression, can accentuate the failure mechanisms associated to local micro-buckling of the fibre.

Internal discontinuities also appear in the laminate in this area of thickness change. They are provoked by the end of a layer, a circumstance habitually referenced in the literature as "ply drop" (Sutherland [1]). An accumulation of these internal defects could favour the appearance and propagation of greater defects.

3.2. Local geometry of stress concentrator

The abrupt transition between the root area and the aerodynamic area generates a local geometry of re-entrant corner, undesirable from a structural point of view since it acts as local stress concentrator.

The root area being the most loaded in the whole blade, the presence of concentrators that amplify the efforts on the laminate results in the existence of critical points for the beginning of failure. The much softer transition that is currently used in modern blades between the root and the aerodynamic areas minimizes these adverse effects.

3.3. Lack of resin and debonding manufacture defects

The joints are the weakest points in all structures. If additionally these joints are associated to the presence of defects, this weakness is consequently accentuated. The corner between the cover, the root and the aerody-

namic area presents manufacture defects associated to the lack of resin (see slice 7) and debonding defects associated to the curing process (see slices 8 and 9).

Although the resin does not have the mechanical properties of the fibres, a laminate with lack of resin does not work as a unique material, its carrying load capacity, mainly under compression, diminishing noticeably. Additionally, defects like those shown in slices 8 and 9 generate delaminations, also undesirable from a structural point of view.

3.4. Evaluation of the problem

Although the reasons set out above do not by themselves fully explain the appearance of the premature failure observed, the combination of the three, in the area of the blade with most stress requirements, can represent sufficient reasons for the premature failure of the blade.

The damage is clearly motivated by a mechanism of fatigue. A prediction of fatigue life is always based on the consideration of a material without defects, the lack of resin and the observed defects accelerating this failure mechanism. Additionally, the combined effect of the geometry of the concentrator and the abrupt change of thickness amplifies the efforts that act locally in an area which in addition to suffering the greatest efforts along the whole blade, presents apparent damage.

The considerable difference in thickness can be motivated either by the abrupt interruption of a longitudinal reinforcement coming from the root or by the overlaps of the circumferential reinforcements, which are also in the root (see Fig. 5). In the first case a softer transition can be obtained with a gradual disappearance of cloths over a greater distance in the longitudinal direction, whereas in the second case it would be sufficient to distribute them appropriately to avoid the accumulation of overlaps at the same position.

The quantitative influence on the fatigue life of the blade of each one of these previously described aspects will be evaluated in the following section. The particular objective is to find, with the knowledge we have about the location of the damage, the approximate period of time before its appearance, and as regards the failure mechanism, under what hypothesis it is reasonable to justify quantitatively a fatigue failure such as the one observed.

4. Justification of the failure

Current knowledge of fatigue failure in laminates of composite materials is, in comparison with metallic materials, certainly limited, due to the more recent development of composites and to their greater complexity, in particular regarding failure mechanisms. A fatigue analysis requires, besides a detailed description of the loads spectrum, a deep knowledge of the fatigue behaviour of the material (Sutherland and Mandell [2]). In this sense the information which is being generated (see for instance DOE/MSU Fatigue Database [3], "Fatigue of materials and components for wind turbine rotor blades" [4]), to simulate the behaviour under fatigue of the materials used in the building of wind turbine blades, is necessary to advance in the analysis and design of these elements.

In this section, the estimation of the fatigue life, in order to elucidate if the detected failure can be justified based on the actual configuration of the blade, will be carried out. The simplified procedure proposed in the

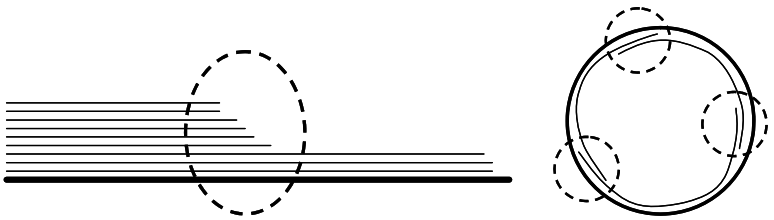

a) longitudinal reinforcements

b) overlaps of the circumferential reinforcements

Fig. 5. Changes of thickness motivated by the reinforcements.

GL standard [5] (which is one of the most extensive and most specific procedures for the design and certification of these elements), will be used. Although more refined treatments for composites fatigue design (Kong et al. [6], Kensche [7], Kong et al. [8], Shokrieh and Rafiee [9]) are available, the GL procedure satisfies the requirements of this study.

4.1. Calculation of fatigue life by means of simplified spectrum according to GL

The GL strength verification adopts the following general expression:

$$S \leqslant \frac{R_k}{\gamma_{mx}} = R_{\mathrm{d}} \tag{4.1}$$

where S, which represents the stress associated to a load case, cannot overcome the design strength R_{d}, which is obtained from decreasing the strength of the material R_k by means of a safety factor that adopts, depending on the case, the values:

$$\text{for the static analysis :} \quad \gamma_{ma} = 2.67 \tag{4.2}$$

$$\text{for the fatigue analysis :} \quad \gamma_{mb} = 1.485 \tag{4.3}$$

The load spectrum to be used could be obtained from real measurements or using simulation techniques. The simplified spectrum shown in Fig. 6, which constitutes a conservative option versus the previous ones, will be used. The range of stresses $\Delta\sigma = |\sigma_{\max} - \sigma_{\min}|$ is represented versus the number of cycles in logarithmic scale, $\log N$, $N_{\max}$ representing an estimation of the blade fatigue life.

Two well differentiated areas can be clearly detected in Fig. 6:

Area a: where a maximum range $\Delta\sigma_{\max} = 1.5 \cdot \bar{\sigma}$ is assumed, $\bar{\sigma}$ being the average value of stresses originated by the aerodynamic forces associated to load case N1.0. The duration in cycles of this part of the spectrum, for a total life of $N_{\max} = 10^x$, is 10^{x-3}.

Area b: which includes the rest of the cycles up to 10^x, with stress ranges according to the equation

$$\Delta\sigma = 0.5 \cdot \bar{\sigma} \cdot \log\left(\frac{N_{\max}}{n}\right) \quad \text{for} \quad \log\left(\frac{N_{\max}}{1000}\right) \leqslant \log n \leqslant \log N_{\max} \tag{4.4}$$

The fatigue life calculation, which of course is made using the most unfavourable value of $\bar{\sigma}$, is based on the S–N curve of the laminate and on the Goodman diagram built from it, Fig. 7. As S–N curves are not available for all the different laminates, and to obtain them experimentally is non-viable from a practical point of view, the GL standard proposes the use of expressions (4.5) and (4.6):

$$\Delta\sigma = \frac{2 \cdot \sigma_{\mathrm{s}}}{\gamma_{mb} \cdot N^{1/9}} \tag{4.5}$$

$$\Delta\sigma^{\mathrm{o}} = \frac{\Delta\sigma}{1 - \frac{\bar{\sigma} \cdot \gamma_{ma}}{\sigma_{\mathrm{s}}}} \tag{4.6}$$

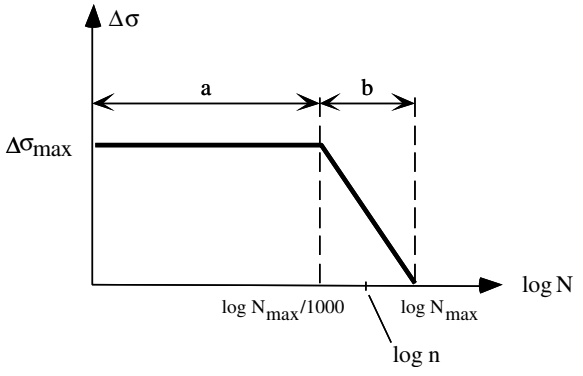

Fig. 6. Simplified spectrum of loads for the calculation of fatigue life.

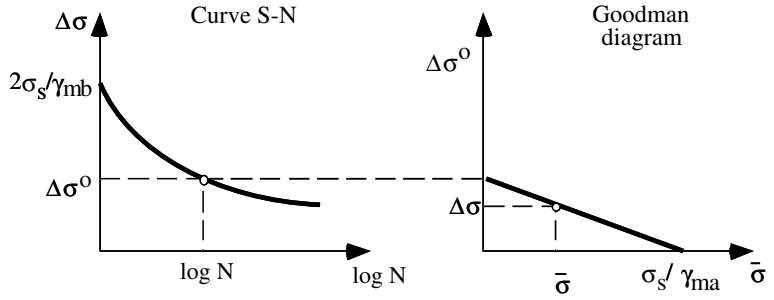

Fig. 7. S–N curve and Goodman diagram.

where σ_s is the laminate strength, N is the number of cycles, $\Delta\sigma = |\sigma_{max} - \sigma_{min}|$ the stress range and γ_{ma} and γ_{mb} are, respectively, the static and fatigue safety factors.

The fatigue life can be calculated using these diagrams, evaluating the accumulated damage D, by the Miner's rule, as

$$D = \sum_i \frac{n_i}{N_i}$$

where n_i is the load cycles number for a stress range i, and N_i is the allowable load cycles number associated to i.

Substituting the expression of the Goodman diagram in the S–N curve, the expression that provides N_i for a determined stress range is obtained

$$N = \left[\frac{2}{\gamma_{mb}} \cdot \left(\frac{\sigma_s}{\Delta\sigma} - \frac{\bar{\sigma} \cdot \gamma_{ma}}{\Delta\sigma}\right)\right]^9 \tag{4.7}$$

The first area of the spectrum (a) with a constant stress range contributes to the accumulated damage with n_1/N_1

$$N_1 = \left[\frac{2}{\gamma_{mb}} \cdot \left(\frac{\sigma_s}{1.5 \cdot \bar{\sigma}} - \frac{\gamma_{ma}}{1.5}\right)\right]^9 \quad n_1 = \frac{N_{max}}{1000} \quad \frac{n_1}{N_1} = 2.6368 \cdot 10^{-3} \cdot \frac{N_{max}}{\left(\frac{\sigma_s}{\bar{\sigma}} - \gamma_{ma}\right)^9} \tag{4.8}$$

The rest of the spectrum contributes with $\int_{\frac{N_{max}}{1000}}^{N_{max}} \frac{dn}{N}$, where introducing the expression of N the following expression can be obtained:

$$\int_{\frac{N_{max}}{1000}}^{N_{max}} \frac{dn}{N} = 4.2824 \cdot 10^{-3} \cdot \frac{N_{max}}{\left(\frac{\sigma_s}{\bar{\sigma}} - \gamma_{ma}\right)^9} \tag{4.9}$$

The complete expression of the accumulated damage is

$$D = 6.919 \cdot 10^{-3} \cdot \frac{N_{max}}{\left(\frac{\sigma_s}{\bar{\sigma}} - 2.67\right)^9} \tag{4.10}$$

an expression which allows the fatigue life corresponding to an accumulated damage equal to $D = 1$ to be calculated. The relationship between the number of cycles and the years of operation for the blades under study is: $14.26 \cdot 10^6$ cycles/year. Using this relationship, the equivalence between cycles and years of life for certain periods of time is shown in Table 2.

Table 2
Equivalence between number of cycles and years

No. of cycles	$0.43 \cdot 10^8$	$0.57 \cdot 10^8$	$0.71 \cdot 10^8$
Years	3	4	5

As is deduced from expression (4.10), in accordance with the simplified treatment adopted, the prediction of fatigue life at a certain point of the blade depends exclusively on the relationship between the strength of the laminate and the value of the average stress existing at this point. Hence, in the following sections, the value of these magnitudes will be analysed in the area affected by the failure.

4.2. Evaluation of the laminate strength

It should be pointed out that when speaking of R_k as the characteristic strength of the material, this refers to the complete laminate. The values of R_k ought to be obtained by testing the different laminates of the blade. This is not practical, due first of all to the number of different stacking sequences of the blade and secondly to the fact that the failure load of most laminates exceeds the load capacity of most conventional testing machines. As an alternative, an empiric rule has been used to evaluate the strength of the laminate working from the strengths of the component layers. This approach has been contrasted with experimental results and with models of progressive failure (Cañas et al. [10]) by means of degradation properties (Tsai [11], Tan [12]), a good agreement being obtained. The expression used is

$$\sigma_{\text{allowable\_}i} = \frac{\sum_n \sigma_{\text{allowable\_}n} \cdot t_{ni}}{t_i} \tag{4.11}$$

where $\sigma_{\text{allowable\_}i}$ is the strength of the i-th laminate, $\sigma_{\text{allowable\_}n}$ is the strength of a layer or a group of layers (the summation extends in n to all layers, or groups, with different strengths: NUFF, DDB, Biaxial 0/90, MAT and balsa wood), t_{ni} is the thickness of material n present in the laminate and finally t_i is the total thickness of the laminate.

Using expression (4.11), with the stacking sequence deduced after the calcination tests (Section 2), and using the allowable values (evaluated experimentally) of each one of the component layers, as well as its thickness, the allowable stress of the laminate corresponding to the section of smaller thickness of slice 5 can be evaluated. The allowable of each layer appears in Table 3. Based on these allowables, a value of 417.1 MPa is obtained for the allowable of the laminate.

It is necessary to consider the appropriate strength value of the laminate to be used in the analysis. To this end, it has to be pointed out that, although the predominant form of work in the area in question is under tension (98%), a certain percentage also takes place under compression (2%). This fact, knowing the different fatigue behaviour under tension and compression, will be taken into consideration in what follows.

A series of compression tests on unidirectional (NUFF) specimens, which is the component that predominantly characterizes the resistant behaviour of the laminates of the blade, were carried out. The specimens were made of a laminate of glass fibre vinylester resin with three layers of NUFF 1450, the total thickness being 3.99 mm. The tests were carried out in an INSTRON 8801 (100 KN). The tested specimens are shown in Fig. 8, the experienced failure type being associated to a phenomenon of micro-buckling of the fibres, which is favoured by the longitudinal waving of the tows of the fibres present in these materials.

The measured average value of the compression strength is 250.9 MPa, presenting a typical deviation of 23.7 and a coefficient of variation of 9.45%. Starting from these values, and applying the statistical treatment that recommends the GL standard, the characteristic value of the compression strength of the NUFF layers would be 189.4 MPa. Therefore, the relationship between the characteristic values of the tensile and compressive strength of the unidirectional (NUFF) layers is 2.65.

Table 3
Allowable values and thicknesses of the different types of layers

Material	$\sigma_{\text{allowable}}$ (MPa)	Thickness (mm)
NUFF (unidirectional)	501.3	$1.333 \cdot 10 = 13.33$
DDB (tri-axial 90/45/−45)	74.1	$1.034 + 0.554 \cdot 2 = 2.142$
DB (bi-axial +45/−45)	112.5	$0.314 \cdot 2 = 0.628$
MAT (random)	124.9	$0.460 + 0.214 = 0.674$

Fig. 8. Compression tests of unidirectional laminates.

Given the predominant character of the unidirectional layers in the resistance in longitudinal direction of the laminate, it would be acceptable to suppose that the relationship between the strength to tension and compression of the laminate follows the same proportion as that corresponding to the layers of NUFF. Based on this hypothesis we can estimate the value of the characteristic compression strength of the laminate under question, which would be 157.4 MPa.

Bearing in mind the fact that part of the life of the element works in tension and another part in compression, the correct treatment would involve using the strengths to tension and compression, respectively, for the corresponding parts of the life of the element. In this case, due to the fact that a simplified spectrum, where it is not possible to distinguish between work in tension and compression, will be used, it has been considered appropriate to modify the value of the allowable stress to be used for the fatigue calculation. To this end, the allowable stress of the laminate will be evaluated as the average value between the tension (417.1 MPa) value and that of compression (157.4 MPa) weighted by the respective work percentages, that is $\sigma_{\text{allowable}} = 411.9$ MPa. It should be pointed out that this small variation in the allowable stress, which could be considered worthless to static effects, has a considerable influence in the fatigue life prediction.

4.3. Evaluation of the average stress of the laminate

The value of the nominal average stress at the neighbourhood of the affected zone has been evaluated by means of a model based on the Strength of Materials Theory (Paluch [13]) that considers the characteristics of the laminates (by means of the classic theory of laminates) and the geometric configuration of the section. The load hypothesis considered is case N1.0 of GL standard. The value of the obtained nominal average stress is: $\bar{\sigma} = 10.77$ MPa. This nominal value can be affected by the change in thickness of the laminate and by the existing concentrator in the transition zone.

The difference in thickness between the adjacent laminates produces an eccentricity of the transferred load which causes the appearance of a bending moment that amplifies the longitudinal normal stress. This effect will be evaluated using the scheme shown in Fig. 9.

The moment $N_x \cdot d$ created by the eccentricity of the load must be absorbed by the laminates. The most unfavourable case is that in which the laminate of smaller thickness absorbs it completely, the maximum normal stress being

$$\sigma_{\max} = \frac{N_x}{e} + \frac{N_x \cdot d}{\frac{1}{12}e^3}\frac{e}{2} = \frac{N_x}{e}\left[1 + 6\frac{d}{e}\right] = \frac{N_x}{e}\left[1 + 6\frac{4.7}{17.9}\right] = \frac{N_x}{e}[1 + 1.57] = 2.57\frac{N_x}{e} \tag{4.12}$$

If, on the other hand, the moment is distributed in the laminates proportionally to their bending stiffness, the minimum value of normal stress for each one of the ends is obtained, its expression being

$$\sigma_{\max} = \frac{N_x}{e} + \frac{1}{6}\frac{N_x \cdot d}{\frac{1}{12}e^3}\frac{e}{2} = \frac{N_x}{e}[1 + 0.26] = 1.26\frac{N_x}{e} \tag{4.13}$$

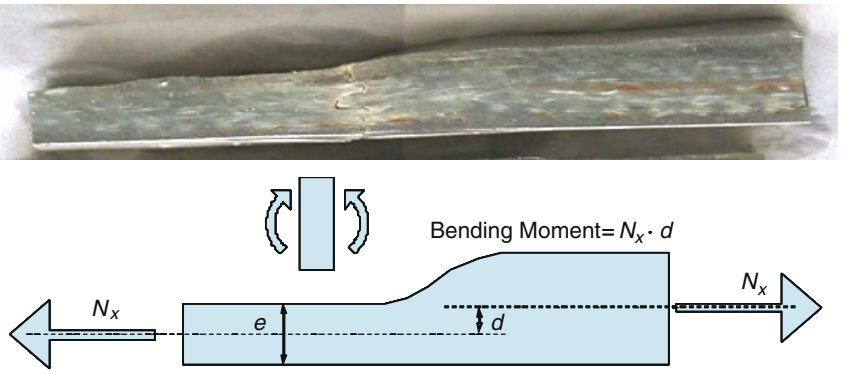

Fig. 9. Evaluation of the influence of the change in thickness.

Therefore, the effect of the change in thickness on the laminates involves an amplification of the normal stress, whose effect can be quantified by a factor, its value being reasonably comprised between 1.26 and 2.57.

With the nominal stress $\bar{\sigma} = 10.77$ MPa and applying the obtained factors, the value of the normal stress would be in the range between 13.6 and 27.7 MPa.

Due to the geometric configuration of the design of the blade, the point under study is within the zone of influence of the concentrator described in Section 3.2, so that the total normal stress would be affected by a concentration factor associated to this geometry. This factor depends on the real configuration of the geometric detail existing at each blade and therefore on the manufacture process. The total normal longitudinal stress is then calculated multiplying the nominal average stress by the factor of amplification due to bending f_{bend} and by the factor of amplification due to the concentrator f_{conc}.

$$\bar{\sigma}_{\text{real}} = \bar{\sigma} \cdot f_{\text{bend}} \cdot f_{\text{conc}} \tag{4.14}$$

Finally, it is necessary to take into consideration that when the laminate is going to suffer the failure of the resistant layer, the external layer presents a crack, motivated by the effect of the concentrator, described in Section 3.2, on the weak laminate of the cover, as is indicated in Fig. 10a.

The effect of this superficial crack on the stress state is double. First, the value of the nominal average stress is increased by the loss of thickness implied by the existence of cracked layers, varying from $\bar{\sigma} = 10.77$ MPa to 11.82 MPa. Secondly, it would imply, strictly speaking, an intensification of the stresses at the tip of the crack. This effect will, for simplicity, be taken as a concentration of the stresses, being included within the factor f_{conc} of expression (4.14).

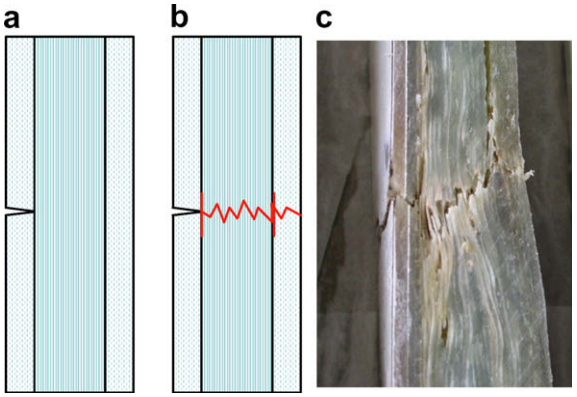

Fig. 10. Scheme of the progression of the crack in the laminate: (a) crack in the superficial layer, (b) crack in the resistant layer, (c) view of the real crack.

4.4. Evaluation of fatigue life

Once the previous considerations have been made, with regard to the laminate strength and the normal longitudinal average stress appearing at the zone of study, an estimation of the fatigue life can be carried out.

Taking expression (4.10), which evaluates the fatigue life, and introducing $\sigma_s = 411.9$ MPa (see Section 4.3) and $N_{max} = 0.71 \cdot 10^8$, corresponding to a life of 5 years (see Table 2), which is approximately the observed life of the blade under study, the values of the average stress that would cause the fatigue failure, that is $D = 1$, can be estimated. The normal longitudinal average stress obtained by means of the described procedure is $\bar{\sigma}_{real} = 59.2$ MPa.

Using expression (4.14), with an average stress of $\bar{\sigma} = 11.82$ MPa, and knowing that the reasonable range of variation of the factor f_{bend} is from 1.26 to 2.57, the factor f_{conc} (due to the geometric concentrator and to the presence of the superficial crack) that causes a real average stress of 59.2 MPa would then be between 1.95 and 3.97.

The obtained values are of a similar order of magnitude to those associated to a geometric concentrator like the one appearing at the root of the blade. In order to evaluate quantitatively the range of values of this concentrator, solutions of similar problems (see Fig. 11a) can be found in the literature (Pilkey [14], pp. 286–287). In particular, two problems with similar geometry to the real concentrator have been taken, corresponding to tension (Fig. 11c) and bending (Fig. 11d) loads.

The parameters on which the stress concentration factor depends can be estimated, for the dimensions of the blade (Fig. 11b), within the following ranges:

$$15 < h/r < 20;\ 0.3 < 2h/D < 0.4$$

where r is the radius of curvature, D and d are the characteristic dimensions at both sides of the concentrator, and h is the difference between D and d.

Using the previous values for the calculation of the stress concentration factor (f_{conc}), the following ranges for the cases of tension and bending are obtained:

$$\text{Tension} : 3.01 < f_{conc} < 3.59$$

$$\text{Bending} : 2.94 < f_{conc} < 3.60$$

The range of values calculated for f_{conc} is, as can be observed, within the interval of values previously obtained (1.95–3.97), values that can reasonably cause the fatigue failure in the period of time considered.

Additionally, using a finite elements model, an estimation of the longitudinal average stress in the zone under study can be obtained, since this point is relatively far from the corner (around 10 cm). The model performed by ANSYS [15] uses shell elements (shell99), which allow orthotropic materials to be used and the stacking sequence of the laminates (up to 100 layers) to be defined. Shell99 is a quadrilateral element of 8

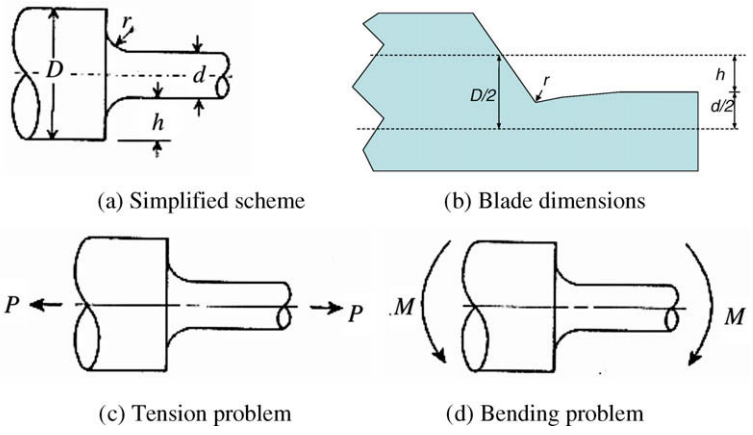

(a) Simplified scheme (b) Blade dimensions

(c) Tension problem (d) Bending problem

Fig. 11. Geometric scheme of the concentrator.

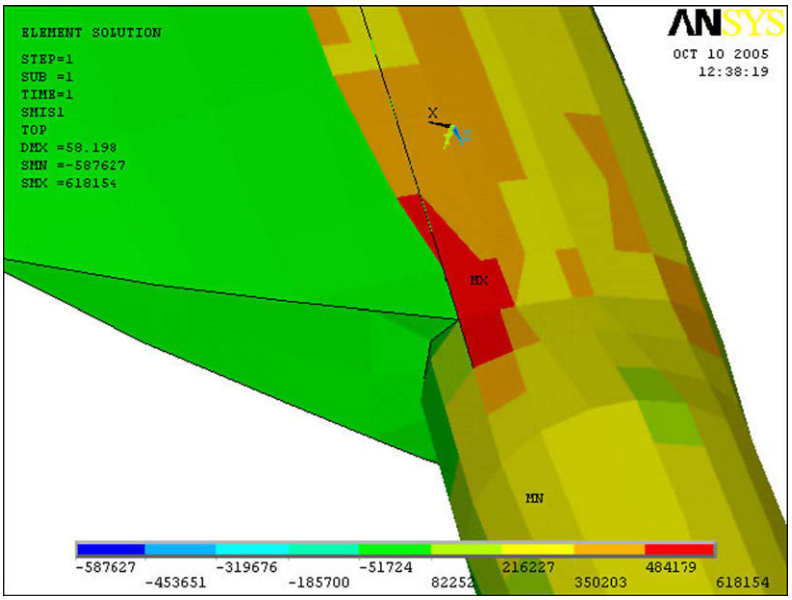

Fig. 12. N_x efforts in the original configuration of the blade.

nodes, 4 in the vertices and 4 at the midpoints of each edge. Each node has 6 degrees of freedom (three displacements and three rotations). The model consists of 5380 nodes and 2027 elements, more than 500 types of different stacking sequences having been defined. The blade has been divided into 64 sections along the longitudinal direction. The nodes at the first section have the displacements restricted, so that the blade is clamped at the root end. This model has been previously validated by mean of comparison with analytical and experimental results [10].

The load case considered for this analysis is N1.0 defined in GL, corresponding to a regular power production. The study carried out is a static analysis of first order (without considering large displacements). The longitudinal normal efforts per unit length (the resultant of the longitudinal normal stresses through the thickness of the laminate) denoted by N_x are represented in Fig. 12.

The value of the longitudinal average stress at the point considered is 26.43 MPa. If this value is compared with the nominal average stress previously evaluated $\bar{\sigma} = 10.77$ MPa (considering that in the numerical model the existence of cracked layers is not contemplated), a stress amplification of 2.45 is obtained, which is within the interval of values previously found (1.95–3.97). This fact corroborates that the actual stress level could reasonably cause the fatigue failure in the period of time considered.

5. Conclusions

The inspection of the blade revealed the following damages:

- Damage appearing in the form of a crack that affected the (non-resistant) superficial laminate, extending over the influence zone of the concentrator and with its likely origin at the corner between the cover and the root.
- Damage in the form of a crack that affected the resistant laminate, extending over the zone where there was an abrupt change in the thickness of the laminate.
- Delamination, lack of bonding, lack of resin and diverse manufacture defects.

The nature of the observed failure seems to be due to a fatigue mechanism. The configuration of the observed cracks seems to indicate that first a superficial crack (Fig. 10a) appeared, probably around the weakest point (corner between the cover and the root) due to the stress concentration, this crack progressing

throughout the superficial layer and inducing delamination between this superficial layer and the resistant laminate. Later on, in the zone where there was an abrupt change of thickness, the presence of the superficial crack together with the effect of the concentrator and the effect of the change in thickness gave rise to the stress state necessary to generate a crack in the resistant laminate (Fig. 10b), which completely broke the laminate, as is observed in Fig. 10c.

By means of the simplified procedure of the standard GL, a calculation of fatigue life for the laminate corresponding to the zone of failure has been carried out. It has been deduced that it is plausible that this laminate reached a fatigue life in the order of 5 years, considering that it was subjected to the combined effect of the presence of the superficial crack, the effect of the geometric concentrator and the effect of the change in thickness, all this giving rise to an amplification of the nominal stress at the zone considered. Additionally, the presence of diverse defects of manufacture could, in any case, contribute to a decrement in the fatigue life of the element.

References

[1] Sutherland HJ. On the fatigue analysis of wind turbines. SAND99-0089, Sandia National Laboratories, Albuquerque, NM; 1999.
[2] Sutherland HJ, Mandell JF. Effect of mean stress on the damage of wind turbine blades. In: 2004 ASME wind energy symposium, AIAA/ASME; 2004. p. 32–44.
[3] Mandell JF, Samborsky DD. DOE/MSU composite material fatigue database: test methods, materials and analysis. SAND97-3002, Sandia National Laboratories, Albuquerque, NM; 1997.
[4] Andersen SI, Bach PW, Bonnee WJA, Kensche CW, Lilholt H, Lystrup A, et al. Fatigue of materials and components for wind turbine rotor blades. European Commission, Directorate-General XII, Science, Research and Development, EUR 16684 EN, Brussels; 1996.
[5] Lloyd Germanischer. Rules and regulations IV – Non Marine Technology, Part I – wind energy. Germanischer Lloyd; 1999.
[6] Kong C, Bang J, Sugiyama Y. Structural investigation of composite wind turbine blade considering various load cases and fatigue life. Energy 2005;30:2101–14.
[7] Kensche CW. Fatigue of composites for wind turbines. Int J Fatigue 2006;28:1363–74.
[8] Kong C, Kim T, Han D, Sugiyama Y. Investigation of fatigue life for a medium scale composite wind turbine blade. Int J Fatigue 2006;28:1382–8.
[9] Shokrieh MM, Rafiee R. Simulation of fatigue failure in a full composite wind turbine blade. Compos Struct 2006;74(3):332–42.
[10] Cañas J, Marín JC, Barroso A, París F. Sobre el uso de modelos de resistencia de materiales y modelos de elementos finitos en el diseño de palas de aerogenerador. In: Proceedings of the MATCOMP-99, Benalmádena (Spain); 1999. p. 271–78 [in Spanish].
[11] Tsai SW. Composites design. Think Composites; 1988.
[12] Tan SC. A progressive failure model for composite laminates containing openings. J Compos Mater 1991;25:556–77.
[13] Paluch B. A software for design and calculation of wind turbine composite rotor blades. European Community Wind Energy Conference, 8–12 March 1993. p. 559–62.
[14] Pilkey WD. Formulas for stress, strain, and structural matrices. John Wiley & Sons Inc.; 1994. p. 286–87.
[15] ANSYS. Swanson Analysis System, Inc.; 2003.